IEEE Access
Multidisciplinary | Rapid Review | Open Access Journal

Received 6 January 2023, accepted 17 January 2023, date of publication 20 January 2023, date of current version 25 January 2023.

Digital Object Identifier 10.1109/ACCESS.2023.3238577

RESEARCH ARTICLE

Compact Slit-Loaded ACS-Fed Monopole Antenna for Bluetooth and UWB Systems With WLAN Band-Stop Capability

MOHSEN KOOHESTANI[1,2], (Senior Member, IEEE), NIMA AZADI-TINAT[3], AND ANJA K. SKRIVERVIK[4]

[1]Department of Electrical and Electronic Engineering, École Supérieure d'Électronique de l'Ouest (ESEO), 49107 Angers, France
[2]Institute of Electronics and Telecommunications of Rennes (IETR), University of Rennes 1, 35042 Rennes, France
[3]Department of Electrical Engineering, Shahrood University of Technology, Shahrood 36199-95161, Iran
[4]Department of Electrical Engineering, Microwave and Antenna Group, École Polytechnique Fédérale de Lausanne (EPFL), 1015 Lausanne, Switzerland

Corresponding author: Mohsen Koohestani (mohsen.koohestani@eseo.fr)

ABSTRACT A compact asymmetric coplanar strip (ACS)-fed monopole antenna is presented, which operates within the Bluetooth and UWB frequency bands with the capability to simultaneously reject the lower WLAN interfering band. The antenna consists of an inverted right triangle patch monopole loaded by open-ended L-shaped slits not only to produce the additional 2.4 GHz passband to the UWB design but also to achieve stopband characteristics around 5.2 GHz. The conceptual equivalent circuit model as well as characteristic mode analyses are carried out in the design evolution process. The proposed antenna has an overall size of only 20 mm × 10 mm, having the smallest area among the so far developed designs, which can be easily integrated within any wireless gadgets. A prototype is fabricated and measured to validate the design, demonstrating the predicted behavior fairly achieved by full-wave analysis. The antenna −10 dB operating bandwidth ranges from 2.38 to 2.42 GHz and from 3.35 to 11 GHz while rejecting from 4.69 to 5.2 GHz. Unlike the unwanted stopband, where the radiation characteristics are adequately deteriorated, the proposed antenna fairly provides stable omni-directional radiation patterns in the *H*-plane, and has an average efficiency (gain) of 87.3% (2.6 dBi) in the desired passband. As far as the antenna transient behavior is concerned, an adequate measured (simulated) system fidelity factor of 0.7 (0.68) is achieved for the transmission of impulse-type UWB signals in the face-to-face configuration.

INDEX TERMS ACS-fed, compact, monopole, Bluetooth, UWB, band-notch.

I. INTRODUCTION

With the exponential pace of technology, portable wireless gadgets with low power consumption, large bandwidth, and more importantly, small dimensions are very attractive in today's competitive market. The two widely-used license-free Bluetooth (2.4-2.48 GHz, 40 channels with 2 MHz spacing) and UWB (3.1-10.6 GHz, over 100% fractional bandwidth) technologies are key enablers for mobile and short-range communications [1], [2]. The evolution of such systems demands the development of compact sized multiband antennas covering both the aforementioned frequency bands.

The design of a single port planar UWB antenna has reached a mature state with most of the recent designs compact in size with a −10 dB lower frequency edge usually around 3 and 4 GHz (Table 1). However, applying conventional techniques, such as inserting a quarter or half guided wavelength parasitic slits into the UWB design, to produce a lower additional resonant frequency around 2.4 GHz would lead to either increased antenna dimensions or potentially deteriorate the performance of the original design due to coupling with other antenna radiating elements. It is even more challenging to simultaneously make such a design

The associate editor coordinating the review of this manuscript and approving it for publication was Sotirios Goudos.

TABLE 1. Comparison among single port Bluetooth/UWB/Multiband planar antennas in literature.

Ref. No.	Excitation Type	Antenna Size (mm³)	-10 dB Operating Bands (GHz)	Band-Reject Function
[10]	Coaxial	13 × 45 × 0.51	2.4/4.3-11	-
[11]	Coaxial	15 × 20 × 1.52	3.3-3.6/4.5-10	-
		43 × 102 × 1.6	2.4-3.6/5.2-6.2/7.1-9	
[12]	CPW	50 × 40 × 0.2	2-10	-
[13]	CPW	31 × 30 × 1.5	2.4/3.5-10	WLAN
[14]	CPW	50 × 45 × 1.59	1.3/2.4-18	WiMAX/WLAN
[15]	CPW	32 × 32 × 0.508	2.4-12.5	WiMAX/WLAN
[16]	CPW	30 × 30 × 1.6	2.4/3.8-11	WLAN
[17]	CPW	25 × 24 × 1.6	1.5/1.8/2.4/3.7-10	WiMAX/WLAN
[18]	CPW	34 × 32 × 1	2-12	WLAN
[19]	CPW	26 × 20 × 0.76	2.4-12	WLAN
[20]	MS	42 × 36 × 1	2.4/3-11	WLAN
[21]	MS	38 × 30 × 1.6	1.8/2.4/3.1-10.6	-
[22]	MS	26 × 30 × 0.8	2.4/3.1-10.6	WLAN
[23]	MS	24 × 17 × 0.787	2.4/3.1-10.6	WiMAX/WLAN/ITU
[24]	MS	40 × 36 × 1	2.2-11	WLAN
[25]	MS	42 × 24 × 1.6	1.8/2.34-2.47/3.1-13	-
[26]	MS	22 × 16 × 1	1.3/1.8/2.4/3.1-10.6	-
[27]	MS	30 × 18 × 1.6	2.28-2.52/3.66-12	WiMAX/WLAN
[28]	MS	42 × 24 × 1.6	2.3-2.5/3.1-12	-
[29]	MS	40 × 40 × 0.8	2.2-10.9	-
[30]	MS	28 × 19 × 0.8	2.4/3.1-10.6	-
[31]	MS	33 × 35.5 × 1	2.4-11	WLAN/ITU
[32]	MS	33 × 40 × 0.8	2.38-14.5	-
[33]	MS	30 × 38 × 1.6	2.4/3.1-13	WLAN
[34]	MS	33 × 27 × 1.5	2.4/3.2-14	-
[35]	MS	26 × 15 × 1.6	2.4/2.95-11.5	-
[36]	MS	40 × 31 × 0.51	2.4/3.5-10	WLAN
[37]	MS	32 × 18 × 0.8	2.4/3-11	-
[38]	ACS	32.5 × 10 × 1.6	2.4/3.2-10.8	-
[39]	ACS	14 × 16 × 1	3.2-11	WiMAX/WLAN
			2.4-2.9/3.6-4.4/5-6	N.A.
[40]	ACS	24 × 10 × 1.6	2.4/5-6.7	N.A.
[41]	ACS	32 × 12 × 1.6	2.4/3.5/5.2/5.58	N.A.
[42]	ACS	27.5 × 13 × 1.6	2.4/3.5/5.05-6.28	N.A.
[43]	ACS	19 × 10 × 1.6	2.5/4.6-6.1	N.A.
This work	ACS	20 × 10 × 1.524	2.4/3.3-11	WLAN

non-responsive to certain frequencies to avoid being interfered by narrowband and higher powered co-existing radio signals, such as the IEEE 802.11 WLAN family around 5.2/5.8 GHz and to achieve a compact size.

The choice of the feeding structure is also an important consideration in designing compact antennas. Coaxial, microstrip (MS) and coplanar waveguide (CPW) transmission lines are the frequently used connection media in printed designs depending on the application. Recently, the asymmetrical coplanar line having a single lateral ground plane compared to the twin lateral grounds in the CPW line, often called asymmetrical coplanar strips (ACS), has attracted the attention of antenna engineers due to leading to smaller designs while adopting similar principles to coplanar transmission line [3]. Among those feeding techniques, the coplanar technology is more popular as it is uniplanar, which offers many well-known advantages such as low dispersion and easy integration with high frequency integrated circuits. It is also preferred in portable and body-worn scenarios due to getting less detuned in proximity to lossy media such as the human body [4], [5]. Some examples of very recent compact UWB studies fed by MS, CPW (grounded CPW) and ACS can be found in [6], [7], [8], and [9], respectively.

The main goal of this study is hence to design a compact coplanar-fed planar multiband antenna, which operates within Bluetooth and UWB frequency bands with the ability to simultaneously reject the lower WLAN interfering band. For this purpose, a comprehensive state-of-the-art study was first carried out considering not only planar antennas covering both the 2.4 GHz and UWB frequency bands [10], [11], [12], [13], [14], [15], [16], [17], [18], [19], [20], [21], [22], [23], [24], [25], [26], [27], [28], [29], [30], [31], [32], [33], [34], [35], [36], [37], [38] but also recently developed compact multiband designs [39], [40], [41], [42], [43] since the intended notch band in the proposed design forms a triband 2.4/3.5/5.5-11 GHz antenna (Table 1). Note that due to the difference in antenna material and dimensions, radiating properties were excluded for a fair comparison. Moreover, since the antenna physical size is the main novel aspect of the work, for each of the considered feeding structures, the conducted review study considers only the smaller antenna structures reported in literature rather than making a comparison with bigger antennas lately developed. The following observations were made: wide

- among the 2.4 GHz/UWB antennas, independently of the feeding structure, the proposed design herein is smaller than the recently developed designs; by 65.8%, 61.5%, 43.2% and 38.4% compared to those presented in [10], [19], [26], and [38], which are fed by coaxial, CPW, MS and ACS, respectively;
- among the multiband designs, where a comparison among previously reported antennas was lately made in [39], the structure in the current work occupies 10.7% less area compared to that in [40]. Note that the smallest ACS-fed multiband design presented in [43] operates at a 4.1% higher frequency while not being able to cover the 3.5 GHz WiMAX (or 5G) deployment band;
- compared to the smallest asymmetrical UWB design [44] (not listed in Table 1 due to not covering the 2.4 GHz band), the size of the proposed antenna is 0.85% smaller. It is worth noting that developing an ACS-fed UWB antenna covering the 2.4 GHz band while being capable to reject a certain interfering band in a compact size has not yet been reported.

The rest of the paper is outlined as follows. Section II presents the antenna design concept and configuration. Section III addresses the experimental results, while concluding contributions of this study are provided in Section IV.

II. ANTENNA DESIGN AND STRUCTURE

A. GEOMETRY

Fig. 1 shows the configurations, design parameters and photograph of the proposed antenna. The monopole comprises an inverted right triangle patch with two truncated L-shaped open-ended slits printed on a 60-mil low-loss Rogers RO4003 substrate (ε_r=3.55, tanδ=0.002). It is fed using the SMA connector, soldered to a 50-Ω ACS feedline with a 3 mm signal strip width and a 0.2 mm gap between the signal strip and the coplanar ground; the SMA connector was considered in the full-wave simulations (Fig. 1a), performed using Ansys HFSS electromagnetic (EM) solver [45]. The backside of the substrate is devoid of metallization. The antenna occupies

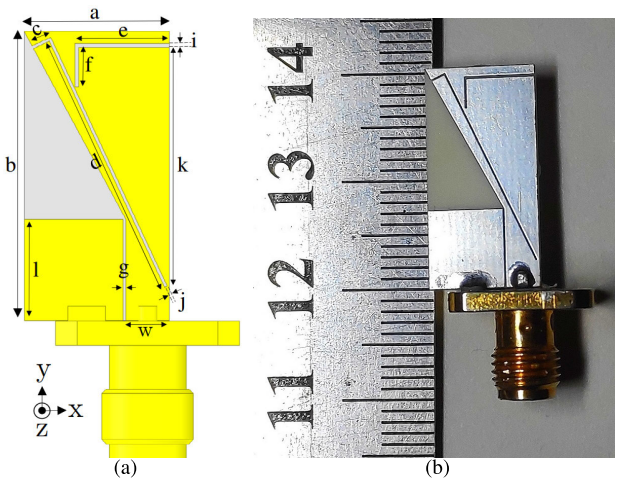

FIGURE 1. Proposed antenna: (a) schematic geometry used in the simulation, (b) prototype photograph; $a = 10$ mm, $b = 20$ mm, $c = 1.4$ mm, $d = 18.8$ mm, $e = 6.5$ mm, $f = 2.75$ mm, $g = 0.2$ mm, $i = 0.25$ mm, $j = 0.2$ mm, $k = 16.5$ mm, $w = 3$ mm, $l = 7$ mm.

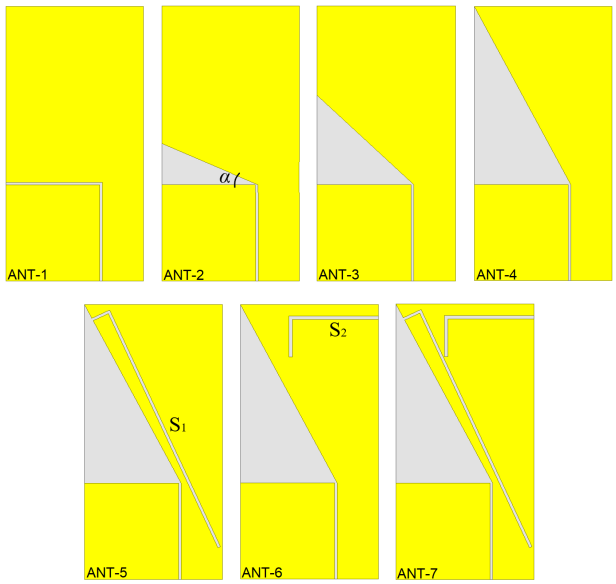

FIGURE 2. Schematic geometry of various antennas involved in the design evolution process. The yellow-colored parts were considered to be copper in the numerical models.

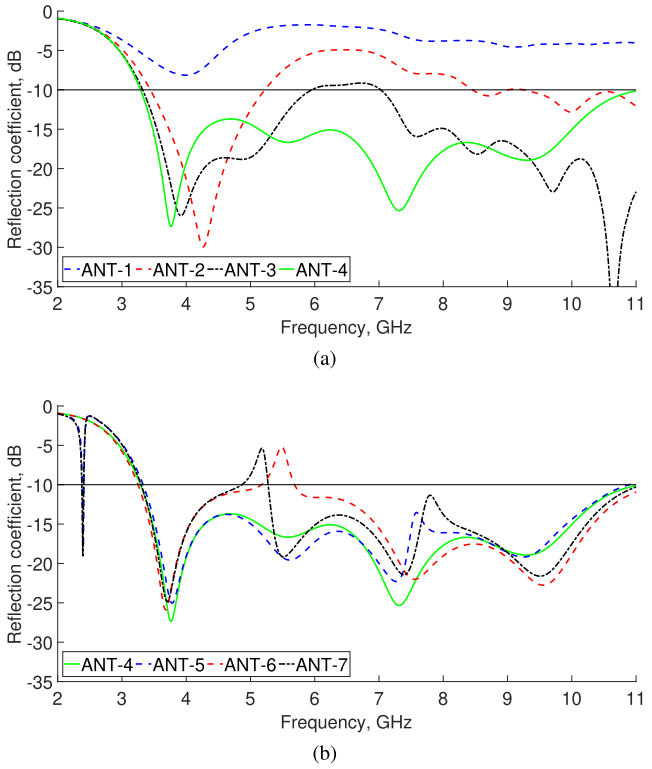

FIGURE 3. Effect of structural modifications shown in Fig. 2 on the antenna input reflection coefficient: (a) ANT-1 to 4, (b) ANT-4 to 7.

an overall area of 20 mm × 10 mm (Fig. 1b), which can be utilized in array or MIMO antenna configurations at a low cost [46].

to achieve the desired antenna performance without increasing the antenna size, weight, complexity or bulkiness.

B. DESIGN EVOLUTION PROCESS

With the aim to show how the antenna was originally designed, the commonly used gradual changing structure technique [47] was employed to achieve the desired antenna performance in limited space without increasing the antenna size, weight, complexity or bulkiness. The miniaturization, adding and subtracting controlled matching bandwidths were reached herein using a proper combination of known techniques and geometries noting that not only preserving the compactness of the antenna but also adjusting desirably its matching bandwidth requires substantial effort, which makes the design innovative (see Table 1). Fig. 2 shows the configurations of the various antennas involved in the design evolution process. Fig. 3 shows, in two sub-figures to avoid the overlap of the curves, the input reflection coefficients of the considered structures.

ANT-1 is the original monopole, which tends to radiate only around 4 GHz (Fig. 3a). The lower left corner of the radiation patch was then gradually truncated by a triangle with the angle 'α' between the hypotenuse and the base (Fig. 2); 'α' for ANT-2 to ANT-4 is 23.2°, 42.8° and 61.4°, respectively. As observed in Fig. 3a, cutting that beveled corner effectively broadens the antenna bandwidth due to modifying the capacitive coupling between the antenna patch and ground plane, consequently neutralizing partially the patch inductive nature to produce nearly pure resistive input impedance across the band of interest; the larger the angle 'α' the greater the −10 dB matching bandwidth. ANT-4 provides an ultra-wide bandwidth ranging from 3.3 to beyond 11 GHz (≃108%) based on $|S_{11}| \leq -10$ dB (Fig. 3a, solid green curve).

Since the lowest operating frequency of ANT-4 is limited to 3.3 GHz, an additional resonator is required to make the antenna operate at a lower frequency to cover the

Bluetooth band. The reflection coefficients of ANT-5 and ANT-6 show that the 2.4 GHz passband can only be due to the inclined L-shaped slit S_1 (Fig. 3b, blue dashed-curve), whereas the horizontal L-shaped slit S_2 produces the stopband around the 5.5 GHz (Fig. 3b, red dashed-curve). It can also be seen that the combination of the two slits into one structure, i.e. ANT-7, leads to the target design to cover the Bluetooth and UWB frequencies while rejecting the lower 5.2 GHz WLAN band (Fig. 3b, black dash-dotted curve). For further insights, the following remarks are worthwhile noting: wide

- the total length of both slits S_1 and S_2 is about $\lambda_g/4$ calculated at the corresponding frequency ($\lambda_g = \lambda_0/\sqrt{\varepsilon_{eff}}$, where $\varepsilon_{eff} = (\varepsilon_r + 1)/2$, λ_g and λ_0 are the guided and free-space wavelengths, respectively); the length of slots S_1 and S_2 is c+d and e+f, respectively, which is approximately $\lambda_g/4$ calculated at 2.4 and 5.2 GHz, respectively. To accommodate the long wavelength slit S_1 into the radiation patch, a small tilt angle with respect to the beveled edge was introduced instead of increasing the width or length of the antenna.
- the addition of the inclined slit S_1 into ANT-4, which forms ANT-5, does not detune the ultra-wide matching bandwidth having a marginal effect on the UWB spectrum (Fig. 3b, blue dashed-curve);
- the addition of the horizontal slit S_2 into ANT-5, which forms ANT-7, results in a slight downshift of the stopband from 5.5 to 5.2 GHz due to the close proximity to the inclined slit S_1 (Fig. 3b, red compared to black dashed-curve). The lower 2.4 GHz band remains unaffected by that proximity keeping the same frequency and reflection coefficient level (Fig. 3b, black dash-dotted-curve).

To sum up, we demonstrated that, while preserving the antenna compactness, the proper addition of the resonating slits to the antenna radiating elements would provide unprecedented degrees of freedom in controlling the produced extra radiating modes either to broaden the antenna matching bandwidth by creating additional resonances or to make the antenna non-responsive to interfering bands by creating notches within its bandwidth. That can be very attractive in designing a more compact antenna without increasing the size, weight, complexity and bulkiness.

C. EQUIVALENT CIRCUIT MODEL ANALYSIS

In order to further explain the operating principle of the two added slits on the UWB performance from the circuit-level point of view, the conceptual equivalent circuit model for the proposed antenna was developed (Fig. 4a). The initial approximate values for the lumped components were defined from the HFSS simulated antenna input impedance (Z_{in}), and the equivalent lumped circuit parameters were then optimized using Keysight advanced design system (ADS) simulations [48].

In Fig. 4a, Z_a represents the complex input impedance of the UWB antenna (ANT-4), which consists of multiple $(1, 2, \ldots, n)$ RLC resonant tanks connected in series [6].

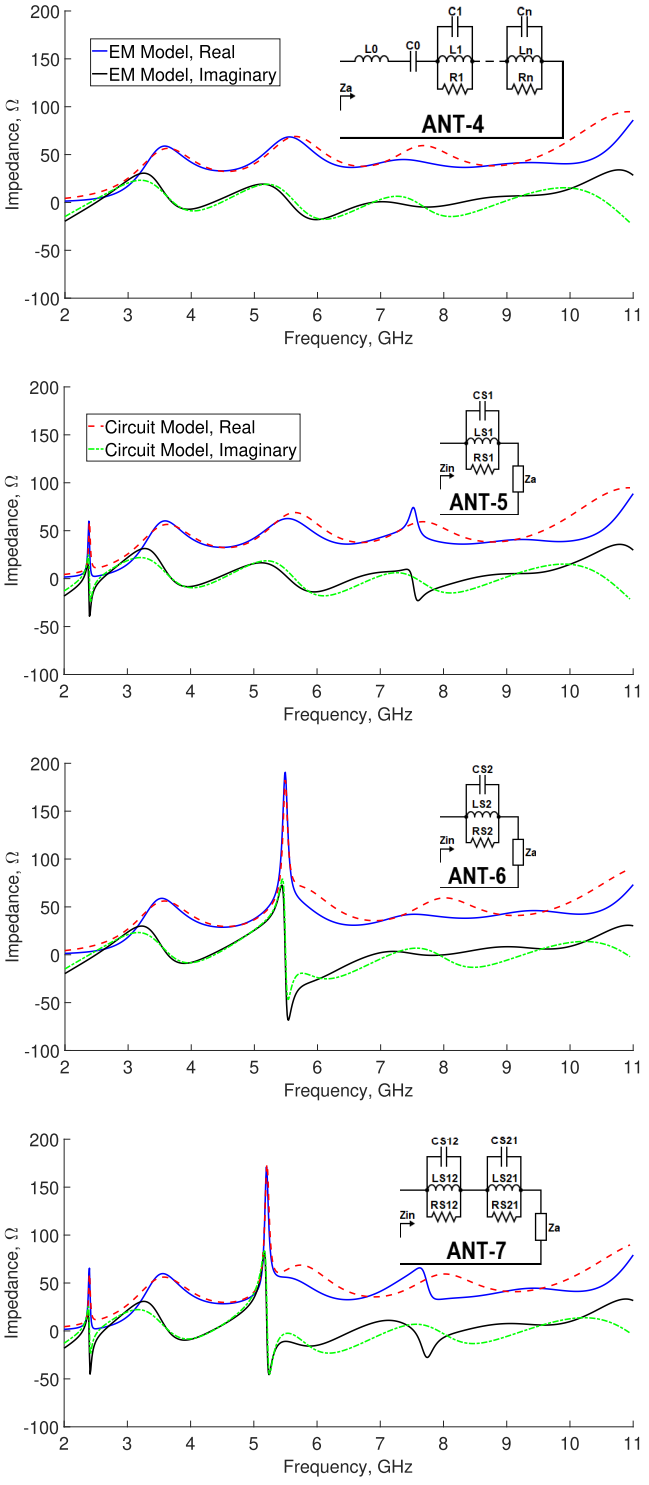

FIGURE 4. Equivalent electrical model and input impedance plots obtained from the EM and circuit models for the various antennas involved in the design evolution process.

In the case of ANT-4, n=4 due to having four adjacent resonant frequencies overlapping with each other (Fig. 3b). Note that the addition of the series capacitor C_0 and inductor L_0 to the RLC circuits is indeed necessary to correctly produce the imaginary part of the antenna input impedance

at the fundamental lower band. To model the two S_1 and S_2 slits, since compared to the UWB reference ANT-4, the real part of ANT-5 and ANT-6 input impedance has a peak value of 60 Ω and 190 Ω both at 2.4 and 5.2 GHz, respectively, while the imaginary part is almost unchanged with the trend from a positive (inductive) to a negative (capacitive) reactance value within the operating bandwidth (Fig. 4), the equivalent circuit diagram can be modeled by a parallel RLC resonant circuit connected in series with Z_a. In a parallel RLC circuit, the input impedance is calculated by $j\omega RL \cdot (R + j\omega L - \omega^2 RLC)^{-1}$, where the resonant frequency is only dependent on the values of the inductor and capacitor $[\omega_0 = (LC)^{-1/2}]$ whereas the bandwidth is controlled by the capacitor and resistor values $[BW = (RC)^{-1}]$ [49]. This explains the slight difference between the inductor, capacitor and resistor values of ANT-6 (LS_2, CS_2 and RS_2) compared to those of ANT-7 (LS_{21}, CS_{21} and RS_{21}) since the addition of the slit S_2 in close proximity to the slit S_1 leads to a slight downshift of the stopband with reduced bandwidth (Fig. 3b). Similar RLC values are expected in the circuit model of ANT-5 (LS_1, CS_1 and RS_1) to ANT-7 (LS_{12}, CS_{12} and RS_{12}) as the presence of slit S_2 alongside with S_1 has no influence neither on the resonant frequency nor on the bandwidth of the 2.4 GHz passband (Fig. 3b).

Fig. 4 compares the input impedance responses for each design step of the proposed antenna obtained from HFSS and ADS for the EM and circuit models, respectively. As observed, the developed equivalent circuit models for ANT-4 to ANT-7 reasonably well predicted the results attained for the antenna EM models. The optimized values obtained for the equivalent circuit models are as follows: L_0=0.16 nH, C_0=1.83 pF, C_1=2.1 pF, L_1=0.36 nH, R_1=57 Ω, C_2=2.6 pF, L_2=0.74 nH, R_2=52 Ω, C_3=2.6 pF, L_3=0.15 nH, R_3=41 Ω, C_4=0.61 pF, L_4=0.32 nH, R_4=90 Ω, CS_1=CS_{12}=95 pF, LS_1=LS_{12}=0.04 nH, RS_1=RS_{12}=51 Ω, CS_2=14.83 pF, LS_2=0.05 nH, RS_2=122 Ω, CS_{21}=14.95 pF, LS_{21}=0.06 nH, RS_{21}=129 Ω.

D. CHARACTERISTIC MODE ANALYSIS (CMA)

Although CMA is usually used in the antenna design phase to systematically achieve the desired performance, for a better understanding of the bandwidth capability and radiation potentials of the two resonant narrow slits inserted into the radiation patch monopole as well as comparing the antenna operation in presence and absence of the excitation port, the modal significance and characteristic angle were also computed for ANT-4 to ANT-7 in the range from 2 to 7 GHz (Fig. 5). This source-free approach not only provides an in-depth physical insight into the antenna design but also makes it possible to explicitly investigate the capability of resonant modes and radiation behavior of the antenna due to being dependent only on the dielectric substrate, and the size and shape of the monopole [50]. In CMA, a mode can be considered strongly resonant when the modal significance is unity and the characteristic angle is equal to 180° [50].

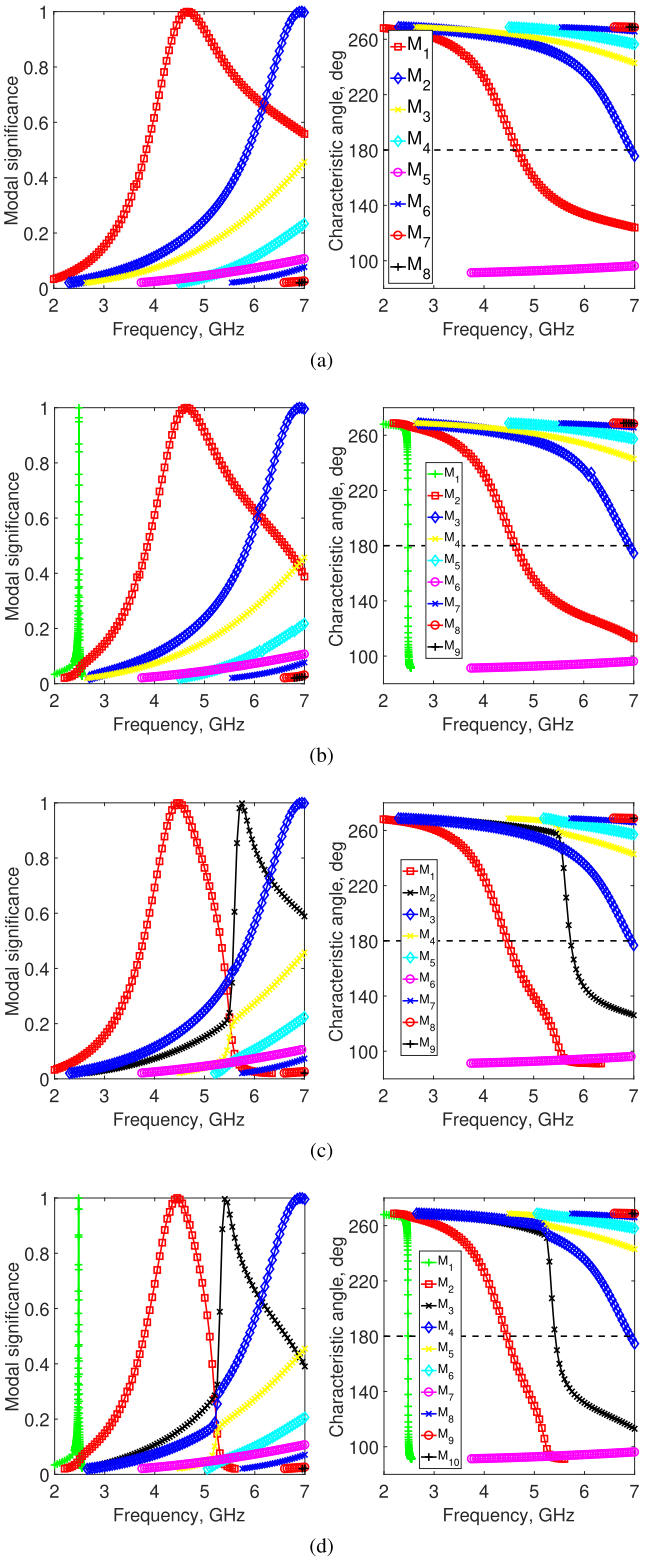

FIGURE 5. Modal significance and characteristic angle variation with frequency for: (a) ANT-4, (b) ANT-5, (c) ANT-6, and (d) ANT-7.

Note that in order to simplify the process, due to the need for huge computational power, zero thickness perfect electric conductors was considered, which can be indeed ignored, the

main objective being the physical interpretation of how the two narrow slits introduced on the patch monopole influence the antenna radiation performance. A review of previous literature shows that such simplifications are very relevant in spite of affecting the accuracy of the modal resonances, where the CMA was usually carried out either without the antenna dielectric material and ground plane or with lossless substrates and zero thickness perfect electric conductors (e.g. [50], [51]). More importantly, it is well-known that all those simplified scenarios have a minor impact on the distribution of eigen currents on the radiating elements [52]. In the full-wave simulations, the minimum modal significance was set to 0.02, meaning that all the modes above that value were calculated.

As observed in Fig. 5a, in the considered frequency range, modes 1 and 2 are dominant in ANT-4 while other modes start to propagate at higher frequencies; the resonant frequency of M_1 and M_2 is at 4.65 and 6.95 GHz, respectively. It can be seen in Fig. 5b that when the slit S_1 is added to ANT-4, an additional resonant mode at 2.49 GHz is produced without disturbing the two initial modes of ANT-4 at 4.65 and 6.95 GHz; the very steep slope in the characteristic angle curve shows the narrowband behavior for that additional mode (green dashed-plus curve). Similarly, as seen in in Fig. 5c, the insertion of the slit S_2 into the ANT-4 structure leads to generate an extra mode at 5.75 GHz. This mode however influences the first dominant mode of ANT-4 resulting in a reduced bandwidth (increased slope steepness of the characteristic angle) and a slight downshift from 4.65 to 4.5 GHz (Fig. 5c, square-red curve). In the final structure of the developed antenna, i.e. ANT-7, all the four main modes are present resonating at 2.48, 4.45, 5.4 and 6.95 GHz (Fig. 5d). As observed, the close proximity of the slit S_2 to S_1 led to a small downshift in the third mode M_3 (from 5.75 to 5.4 GHz) and consequently in the second mode M_2 (from 4.5 to 4.45 GHz). All these port-independent results are perfectly in line with the behavior of antennas ANT-4 to ANT-7 when they are fed at the port of feeding line (see the explanations provided for Fig. 3b).

E. MODAL CURRENT DISTRIBUTION

To further demonstrate the antenna operation with aim to highlight the role of the two resonant slits, the surface current distributions derived from the eigenvectors were computed for ANT-4 to ANT-7 (Fig. 6). The colors representing the current distribution intensity go from dark blue (weak current density) to green, yellow and to red (strong current density). For the sake of comparison, the vector currents in ANT-4 were monitored at the resonant modes of ANT-7 to support the explanations, whereas for ANT-5 and ANT-6 they were simulated at the produced dominant mode frequency due to the narrow slits.

A first look at the results in Fig. 6d and 6e indicates that both slits S_1 and S_2 efficiently radiate due to the large amount of currents mainly concentrated around the slits at their corresponding dominant mode frequency. Moreover, the flow and

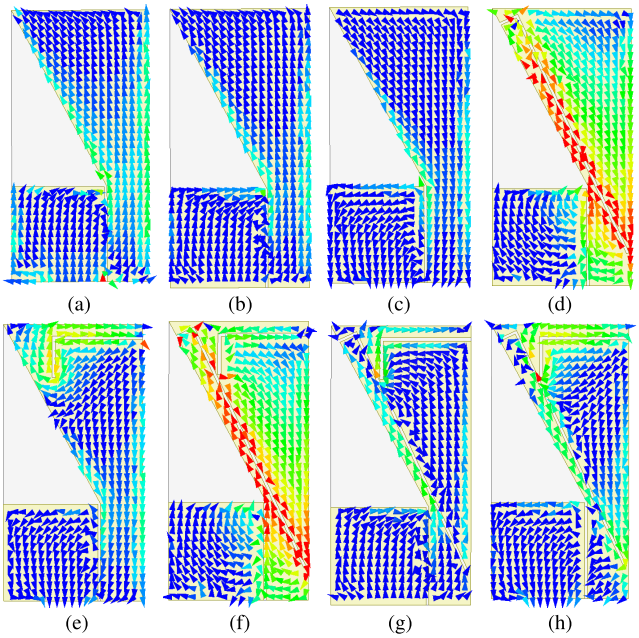

FIGURE 6. Modal current distributions: (a)-(c) ANT-4 at 2.48, 4.45 and 5.4 GHz, respectively, (d) ANT-5 at 2.49 GHz, (e) ANT-6 at 5.75 GHz, and (f)-(h) ANT-7 at 2.48, 4.45 and 5.4 GHz, respectively. Scale: logarithmic with 15 subdivisions ranging from 1E1 to 1E3 A/m.

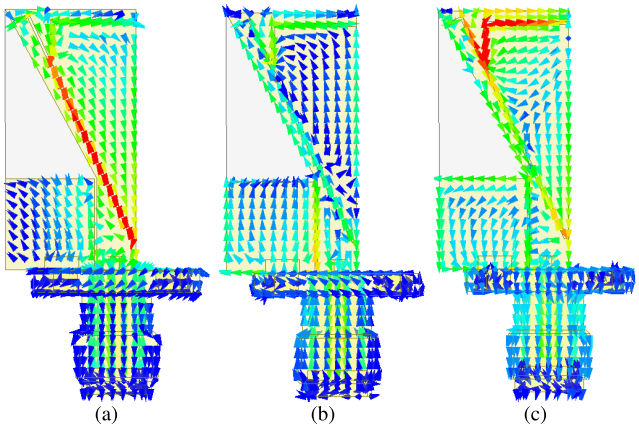

FIGURE 7. Surface current distributions on ANT-7 at: (a) 2.4 GHz, (b) 3.7 GHz, and (c) 5.2 GHz. Scale: logarithmic with 15 subdivisions ranging from 1E0 to 1E3 A/m for an input power of 1 W.

oppositely-directed currents along the slits, which are similar to those in transmission lines, indicate that the maximum current at the end of both slits (low impedance or short circuit) is transformed to high impedance (open circuit) at the other end due their approximate $\lambda_g/4$ length. The location of low and high impedances on the radiation patch indicates the impact of the large currents produced by the two open-ended slits on the excited surface currents in the antenna.

Comparing the currents in Fig. 6a and 6f shows that in the close proximity of the resonating slit S_1, the privileged current direction on the radiation patch orients similarly to that along the slit. Although there is a large oppositely-directed current toward the antenna feed point and the currents near the base

of the monopole are reoriented, since the original antenna (ANT-4) does not radiate around 2.4 GHz, the impact on the antenna excited surface currents cannot be destructive at that frequency. Instead, the high amount of current all around the patch and partly on the ground, which is strong enough to even redirect the currents, clearly reveals that the antenna is resonant at that frequency.

Comparing the currents at the 4.45 GHz passband in presence and absence of the slits, shown in Fig. 6b and 6g, illustrates the marginal impact of the slit S_1 on the current direction over the patch and coplanar ground. However, the variation in the orientation of the currents at the top of the patch near the slit S_2 indicates the influence of the latter on the antenna behavior. This further explains the slight downshift of the antenna dominant mode (Fig. 5c compared to 5a) and notch band (Fig. 3b, red curve compared to back curve) when the slit S_2 was inserted in the patch.

Comparing the currents in Fig. 6c and 6h shows that the slit S_2 creates a large current, which in its close proximity, the currents on the patch also tends to orient along the same direction. The amount of the currents flowing towards the antenna port are large enough to highly disturb and deform the currents approaching the feed point. Therefore, destructive interference with the excited surface currents can be expected, which makes the antenna non-responsive at that frequency.

All the above results clearly validate the design concept of the proposed antenna. A very similar behavior in the surface current distributions can be seen in Fig. 7 when the antenna was fed through the SMA (of course at the right frequencies) compared to those obtained from the characteristic mode theory at each of the considered frequencies; the current directions shown in Fig. 6f to 6h, not only on the patch monopole but also on the coplanar ground plane, fairly agree well with those illustrated in Fig. 7a to 7c, respectively. This further indicates the appropriate feeding location to obtain the intended radiation properties. Additionally, the electric currents mostly concentrated on the edge portions of the S_1 and S_2 slits at 2.4 and 5.2 GHz, respectively, indicate that those elements have the most significant influence on the antenna operation at those frequencies. Hence, the bandpass and bandstop resonances can be precisely controlled by adjusting the corresponding slits dimensions.

F. PARAMETRIC STUDY

The key parameters influencing the added (2.4 GHz) and subtracted (5.2 GHz) resonant frequencies are the lengths and positions of the slits S_1 and S_2. In order to demonstrate that, Fig. 8 showcases the input reflection coefficient of the antenna as function of the slits parameters.

A first look at the results reveals that any variations in the dimensions of each slit strongly influence the corresponding resonant frequency (S_1 and S_2 resonant modes vary in the range between 2-3 GHz and 5-6 GHz) with hardly any impact on the other mode frequency (Fig. 8). A closer look indicate that the length and width of each of the slits S_1 and S_2 can be adjusted to precisely adjust their resonances within the antenna matching bandwidth. Therefore, by appropriately tuning the resonator dimensions, the two additional bandpass and bandstop can be achieved at desired frequencies.

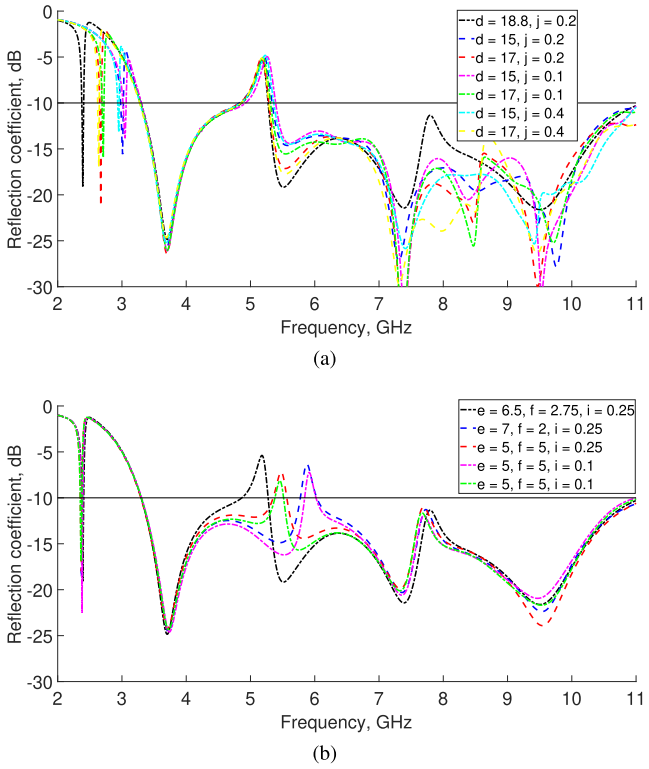

FIGURE 8. Simulated antenna input reflection coefficients as a function of the slits parameters: (a) S_1, (b) S_2.

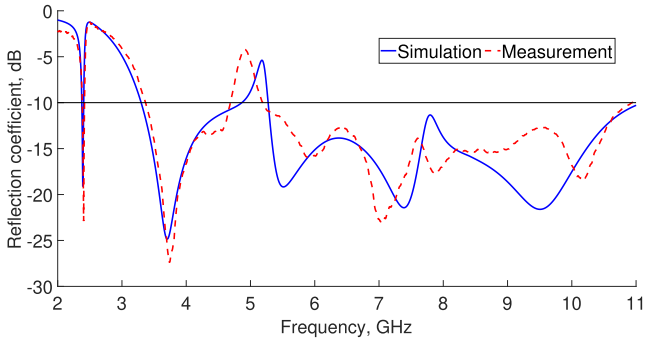

FIGURE 9. Measured and simulated reflection coefficient of the proposed antenna.

III. RESULTS AND DISCUSSION

To validate the proposed design, a prototype of the antenna was fabricated, and measured results in terms of input reflection coefficient, far-field radiation patterns in the two main E- and H-planes, total efficiency and peak realized gain at several frequencies of the desired passbands and the unwanted stopband are presented. The antenna time domain radiation properties in terms of impulse response and system fidelity factor are also reported.

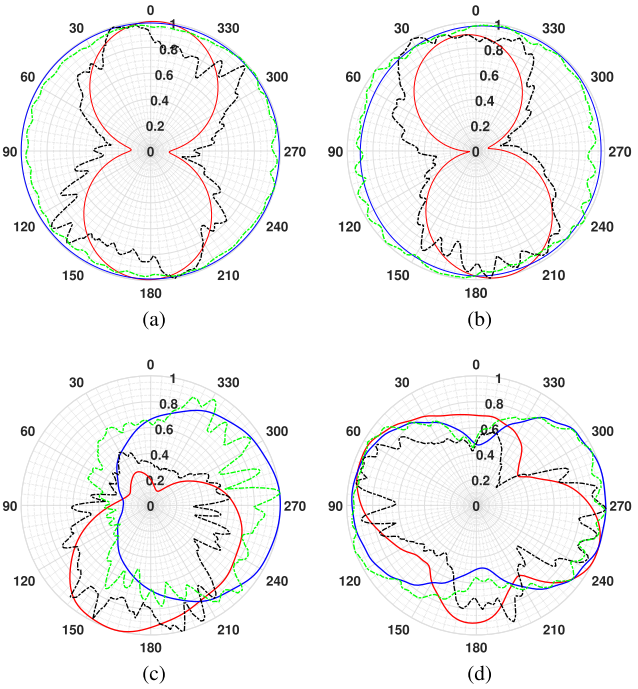

FIGURE 10. Measured and simulated normalized radiation patterns of the proposed antenna at: (a) 2.4 GHz (lower passband frequency), (b) 3.7 GHz (middle passband frequency), (c) 4.9/5.2 GHz (stopband frequency), and (d) 9.5 GHz (higher passband frequency). Dashed-black (solid-red) and dashed-green (solid-blue) are the measured (simulated) *E*- and *H*-plane, respectively.

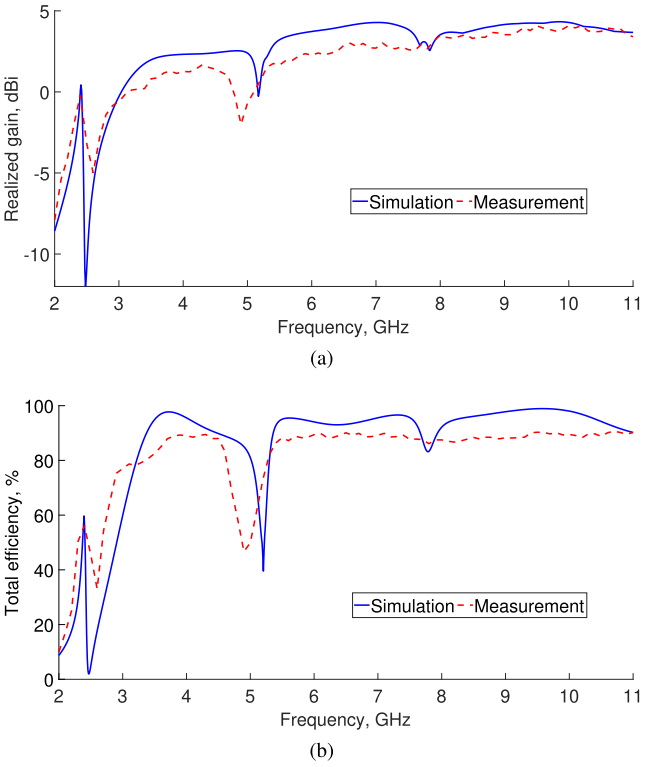

FIGURE 11. Measured and simulated (a) realized gain, and (b) total efficiency of the proposed antenna.

Fig. 9 plots the simulated and measured antenna reflection coefficients demonstrating a fairly good agreement between the results. The antenna −10 dB bandwidth ranges from 2.38 to 2.42 GHz and from 3.35 to 11 GHz while rejecting from 4.69 to 5.2 GHz ($|S_{11}|_{max} = -4.9$ dB, which is equivalent to VSWR 3.6). These results confirm that the proposed antenna not only operates within both the Bluetooth and UWB frequency bands but also is capable to reject the lower WLAN band within its matching bandwidth.

Fig. 10 depicts the measured and simulated normalized far-field radiation patterns of the proposed antenna, in both *E*-plane (*y*-*z*) and *H*-plane (*x*-*z*), at three different representative passband frequencies (2.4, 3.7 and 9.5 GHz) and at the stopband frequency (4.9 GHz in experiments and 5.2 GHz in simulations). Although the cable currents caused the ripples in the measured patterns, a reasonably good agreement between the measurement and simulation results was achieved. As seen in Fig. 10a, 10b, and 10d, in the considered passbands, the antenna exhibits nearly omni-directional and fairly bidirectional coverage in the *H*- and *E*-plane, respectively; the radiation properties are relatively stable in the operating bands and the slight tilt in the *E*-plane is known to be due to the asymmetric coplanar ground. However, the highly deteriorated radiation characteristics observed in the unwanted stopband (Fig. 10c) demonstrate the rejection capability of the proposed antenna; a fact is corroborated in [53].

Fig. 11a plots the measured and simulated antenna peak realized gains as a function of frequency; experiments were conducted with a 100 MHz step. As observed in the figure, the measured results reasonably follow the numerical ones. The antenna gain within the entire band of interest vary from 1 to 4.1 dBi, except at the 2.4 GHz passband and the 4.9/5.2 GHz stopband; the measured (simulated) gain values at 2.4 and 4.9/5.2 GHz are −0.2 (0.43) dBi and −2 (−0.27) dBi, respectively. The measured antenna average gain from 3.3 to 4.7 GHz and from 5.2 to 11 GHz is 1.1 and 3.1 dBi, respectively. In the 2.4 GHz band, the limited antenna gain is explained by the significant amount of oppositely-directed high intensity current along the slit S_1 (Fig. 7a), which causes ohmic losses. Although the latter effect is nearly unavoidable in miniature antennas, the in-band gain of the proposed antenna is considered adequate for practical low power applications, whereas the significant gain decrease (roughly from 1 down to −2 dBi in experiment and from 2.5 to −0.3 dBi in simulation) in the stopband can sufficiently eliminate possible disturbances from other co-existing systems.

Fig. 11b exhibits the measured and simulated total efficiency of the proposed antenna, showing a good agreement between the results. As it can be seen, an average efficiency of over 87.3% across the entire antenna band of interest was achieved, except at 2.4 and 4.9/5.2 GHz bands; the measured (simulated) efficiency values at 2.4 and 4.9/5.2 GHz are approximately 56.1% (59.7%) and 46.7% (39.6%), respectively. That efficiency value at 2.4 GHz can be explained by the high intensity oppositely directed currents around the slit

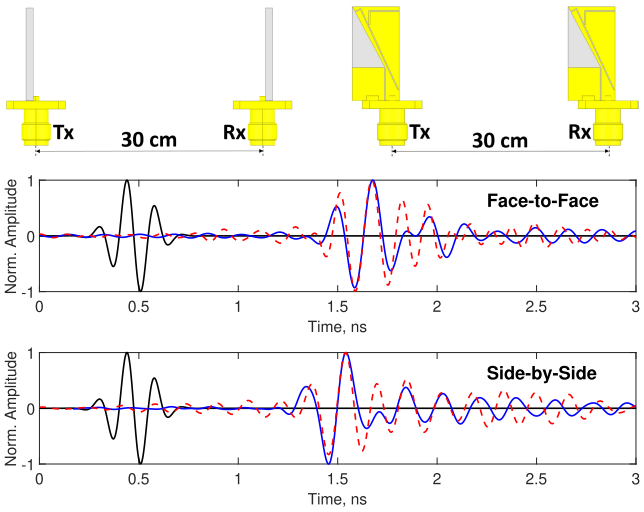

FIGURE 12. Measured and simulated Tx and Rx signals of the proposed antenna: input (solid-black), simulated (solid-blue), measured (dash-red).

S_1 (Fig. 7a). The sharp efficiency drops in the vicinity of the stopband (from 87% down to 46.7% in measurement and from 86% to 39.6% in simulation) causes adequate deterioration in the radiation properties in the band.

For the transmission of impulse-type UWB signals, the transient response of the proposed antenna was also investigated to assess the pulse distortion in the received signals. To quantify the level of distortion, the system fidelity factor (*SFF*) [54], which reflects the correlation between the transmitted (Tx) and the received (Rx) time signals, was calculated for a Gaussian input pulse rather than fidelity factor (*FF*) due to being a measurable quantity [55]. The measurement setup makes use of two identical antennas in face-to-face and side-by-side configurations with 30 cm distance in between to validate the far-field condition, as can be seen in Fig. 12.

Fig. 12 shows the simulated and measured Tx and Rx time signals of the proposed antenna demonstrating a reasonable prediction of the antenna transient response for the considered configurations; the measured (simulated) *SFF* of the antenna is about 0.7 (0.68) and 0.66 (0.62) for the face-to-face and side-by-side cases, respectively. The ringing distortions observed in the impulse response in simulations and measurements is due to the impedance mismatch at the stopband; a fact corroborated in [53]. Although the antenna compact dimensions impacts its transient behavior, the level of pulse distortion is considered acceptable (*SFF*>0.5 [54], [55]), which is suitable for the use in the impulse-type UWB systems. It is worth noting that since *SFF* takes into account the amount of distortion induced by both the Tx and Rx antennas, it would always have smaller values compared to *FF* as well as *FF* of the system [56].

IV. CONCLUSION

A compact multiband planar monopole antenna for Bluetooth and UWB applications was proposed with band rejection characteristics around the IEEE 802.11 WLAN family. The antenna has a simple structure and is fed by an asymmetric coplanar strip, where the overall area is only 10 mm × 20 mm, the smallest so far reported, which can be easily integrated with any smart wireless device for portable IoT applications. Two L-shaped open-ended slits were introduced in the patch monopole not only to produce the additional 2.4 GHz band to the original UWB design but also to simultaneously create the stopband around 5.2 GHz. The conceptual equivalent electrical model for the proposed antenna was developed to explain the operating principle of the slits on the UWB performance from the circuit-level point of view. The theory of characteristic mode was also applied for the physical interpretation of the radiation mechanism of the loaded slits on the antenna design process.

Measured results confirmed that the proposed antenna has suitable characteristics for reliable wireless communications. The antenna −10 dB operating bandwidth covers from 2.38 to 2.42 GHz and from 3.35 to 11 GHz, in which there is a notched band from 4.69 to 5.2 GHz. In the desired passbands, the antenna provides almost omnidirectional radiation patterns in the *H*-plane, radiates efficiently (87.3% on average) with acceptable gains (2.6 dBi on average). The deteriorated antenna radiation properties, in terms of pattern, gain and efficiency, in the stopband demonstrated the capability of the antenna to effectively reject the out-of-band interference signals. For the transmission of impulse-type UWB time signals, the proposed antenna demonstrated an acceptable transient performance with system fidelity factors of 0.7 and 0.66 in face-to-face and side-by-side configurations, respectively. Therefore, the proposed antenna is a very competitive candidate for future Bluetooth and UWB modern applications.

ACKNOWLEDGMENT

The authors would like to cordially thank Dr. A. Moknache from Ansys technical support team, Paris, France, for the fruitful discussions.

REFERENCES

[1] C. Saha, J. Y. Siddiqui, and Y. M. M. Antar, *Multifunctional Ultrawideband Antennas: Trends, Techniques, and Applications*. Boca Raton, FL, USA: CRC Press, 2019.
[2] G. Kumar and K. P. Ray, *Broadband Microstrip Antenna*. Norwood, MA, USA: Artech House, 2003.
[3] V. Deepu, R. K. Raj, M. Joseph, M. N. Suma, and P. Mohanan, "Compact asymmetric coplanar strip fed monopole antenna for multiband applications," *IEEE Trans. Antennas Propag.*, vol. 55, no. 8, pp. 2351–2357, Aug. 2007.
[4] M. Koohestani, N. Pires, A. K. Skrivervik, and A. A. Moreira, "Bandwidth enhancement of a wearable UWB antenna near a human arm," *Microw. Opt. Technol. Lett.*, vol. 55, no. 12, pp. 2965–2967, Dec. 2013.
[5] M. Koohestani, A. A. Moreira, and A. K. Skrivervik, "Feeding structure influence on performance of two UWB antennas near a human arm," in *Proc. 8th Eur. Conf. Antennas Propag. (EuCAP)*, Apr. 2014, pp. 834–836.
[6] S. Doddipalli and A. Kothari, "Compact UWB antenna with integrated triple notch bands for WBAN applications," *IEEE Access*, vol. 7, pp. 183–190, 2019.
[7] A. J. A. Al-Gburi, I. B. M. Ibrahim, M. Y. Zeain, and Z. Zakaria, "Compact size and high gain of CPW-fed UWB strawberry artistic shaped printed monopole antennas using FSS single layer reflector," *IEEE Access*, vol. 8, pp. 92697–92707, 2020.

[8] S. Park and K.-Y. Jung, "Novel compact UWB planar monopole antenna using a ribbon-shaped slot," *IEEE Access*, vol. 10, pp. 61951–61959, 2022.

[9] C. S. Rajan, K. A. Ansal, C. S. Ragamalika, and M. Sreenath, "Meander slotted ACS fed antenna with stepped ground plane for UWB applications," in *Proc. 2nd Int. Conf. Adv. Comput., Commun., Embedded Secure Syst. (ACCESS)*, Sep. 2021, pp. 13–17.

[10] Z. Ning Chen, D. Liu, and B. Gaucher, "A planar dualband antenna for 2.4 GHz and UWB laptop applications," in *Proc. IEEE 63rd Veh. Technol. Conf.*, May 2006, pp. 2652–2655.

[11] C. T. P. Song, S. Ooi, and B. Koh, "Planar dual mode antenna for 2.4 GHz and UWB," in *Proc. IEEE Antennas Propag. Soc. Int. Symp.*, Jul. 2008, pp. 1–4.

[12] D. Gaetano, P. McEvoy, M. Ammann, C. Brannigan, L. Keating, and F. Horgan, "Footwear and wrist communication links using 2.4 GHz and UWB antennas," *Electronics*, vol. 3, no. 2, pp. 339–350, Jun. 2014.

[13] M. Rahman, M. NagshvarianJahromi, S. S. Mirjavadi, and A. M. Hamouda, "Compact UWB band-notched antenna with integrated Bluetooth for personal wireless communication and UWB applications," *Electron.*, vol. 8, no. 2, pp. 158–171, 2019.

[14] S. Kumar, R. Kumar, and R. Vishwakarma, "A circular disc microstrip antenna with dual notch band for GSM/Bluetooth and extended UWB applications," *Int. J. Eng. Technol.*, vol. 7, no. 2.16, pp. 11–18, 2018.

[15] A. Wu and B. Guan, "A compact CPW-fed UWB antenna with dual band-notched characteristics," *Int. J. Antennas Propag.*, vol. 2013, pp. 1–7, Jan. 2013.

[16] N. M. Awad and M. K. Abdelazeez, "Bluetooth/UWB circular patch antenna with dual band notches," in *Proc. IEEE Jordan Conf. Appl. Electr. Eng. Comput. Technol. (AEECT)*, Dec. 2013, pp. 1–4.

[17] Y.-L. Luo, L. Xu, Z.-Y. Xin, and S. He, "A compact CPW-FED UWB antenna with GSM, GPS, Bluetooth and dual notch bands applications," *Prog. Electromagn. Res. C*, vol. 35, pp. 205–219, 2013.

[18] A. C. Shagar and S. D. Wahidabanu, "Novel wideband slot antenna having notch-band function for 2.4 GHz WLAN and UWB applications," *Int. J. Microw. Wireless Technol.*, vol. 3, no. 4, pp. 451–458, Aug. 2011.

[19] Y. K. Soni and N. K. Agrawal, "Compact UWB/Bluetooth integrated uniplanar antenna with WLAN notch property," in *Proc. ICT Crit. Infrastruct., 48th Annu. Conv. Comput. Soc. India*, in Advances in Intelligent Systems and Computing, vol. 248. Cham, Switzerland: Springer, Cham, 2014, pp. 459–466.

[20] Z. Han, Z. Ma, and Q. Xue, "Integrated Bluetooth and UWB antenna with single band-notched," *ACES J.*, vol. 30, no. 8, pp. 838–843, 2015.

[21] S. D. Mahamine and R. P. Labade, "A design of integrated GSM and Bluetooth ultra wide band printed monopole antenna (UWB) for wireless applications," in *Proc. IEEE Bombay Sect. Symp. (IBSS)*, Sep. 2015, pp. 1–6.

[22] L. Xu, Y.-L. Luo, and Z.-Y. Xin, "A compact monopole antenna for Bluetooth and UWB applications with dual band notched characteristics," in *Proc. Int. Workshop Microw. Millim. Wave Circuits Syst. Technol.*, Oct. 2013, pp. 50–53.

[23] G. S. Reddy, A. Kamma, S. K. Mishra, and J. Mukherjee, "Compact Bluetooth/UWB dual-band planar antenna with quadruple band-notch characteristics," *IEEE Antennas Wireless Propag. Lett.*, vol. 13, pp. 872–875, 2014.

[24] Y.-B. Yang, F.-S. Zhang, F. Zhang, L. Zhang, and Y.-C. Jiao, "Design of novel wideband monopole antenna with a tunable notched-band for 2.4 GHZ WLAN and UWB applications," *Prog. Electromagn. Res. Lett.*, vol. 13, pp. 93–102, 2010.

[25] G. Li, H. Zhai, T. Li, X. Y. Ma, and C.-H. Liang, "Design of a compact UWB antenna integrated with GSM/WCDMA/WLAN bands," *Prog. Electromagn. Res.*, vol. 136, pp. 409–419, 2013.

[26] A. Foudazi, H. R. Hassani, and S. M. A. Nezhad, "Small UWB planar monopole antenna with added GPS/GSM/WLAN bands," *IEEE Trans. Antennas Propag.*, vol. 60, no. 6, pp. 2987–2992, Jun. 2012.

[27] L. Xiong and P. Gao, "Dual-band planar monopole antenna for Bluetooth and UWB applications with WiMAX and WLAN band-notched," *Prog. Electromagn. Res. Lett.*, vol. 28, pp. 183–194, 2012.

[28] S. K. Mishra, R. K. Gupta, A. Vaidya, and J. Mukherjee, "A compact dual-band fork-shaped monopole antenna for Bluetooth and UWB applications," *IEEE Antennas Wireless Propag. Lett.*, vol. 10, pp. 627–630, 2011.

[29] J. Ren, D. Mi, and Y.-Z. Yin, "Compact ultrawideband MIMO antenna with WLAN/UWB bands coverage," *Prog. Electromag. Res. C*, vol. 50, pp. 121–129, 2014.

[30] J. H. Bae, J. G. Jeong, Y. J. Yoon, and Y. Kim, "A compact monopole antenna for Bluetooth and UWB applications," in *Proc. Int. Symp. Antennas Propag.*, 2017, pp. 1–2.

[31] F.-T. Zha, S.-X. Gong, G. Liu, H.-Y. Yang, and S.-G. Lin, "Compact slot antenna for 2.4 GHz/UWB with dual band-notched characteristic," *Microw. Opt. Technol. Lett.*, vol. 51, no. 8, pp. 1859–1862, Aug. 2009.

[32] Y. Y. Sun, S. W. Cheung, and T. I. Yuk, "An ISM/UWB antenna with offset feeding and slotted ground plane for body-centric communications," *J. Elec. Electron. Eng.*, vol. 1, no. 2, pp. 45–50, 2013.

[33] R. Labade, S. Deosarkar, N. Pisharoty, and A. Malhotra, "Compact integrated Bluetooth UWB bandnotch antenna for personal wireless communication," *Microw. Opt. Technol. Lett.*, vol. 58, no. 3, pp. 540–546, Mar. 2016.

[34] A. Khurshid, J. Dong, and R. Shi, "A metamaterial-based compact planar monopole antenna for Wi-Fi and UWB applications," *Sensors*, vol. 19, no. 24, p. 5426, Dec. 2019.

[35] F. Jiang and D.-K. Park, "Compact microstrip feed dual band monopole antenna for UWB and Bluetooth applications," *J. Korean Soc. Mar. Eng.*, vol. 41, no. 10, pp. 1024–1028, Dec. 2017.

[36] M. Elhabchi, M. N. Srifi, and R. Touahni, "A novel dual band hexagonal antenna for Bluetooth and UWB applications with single band notched," *Adv. Electromagn.*, vol. 7, no. 5, pp. 63–68, Nov. 2018.

[37] L. Xu, B. Yuan, and S. He, "Design of novel UWB slot antenna for Bluetooth and UWB applications," *Prog. Electromag. Res. C*, vol. 37, pp. 211–221, 2013.

[38] Y.-F. Liu, P. Wang, and H. Qin, "Compact ACS-fed UWB monopole antenna with extra Bluetooth band," *Electron. Lett.*, vol. 50, no. 18, pp. 1263–1264, 2014.

[39] A. Kumar, P. Naidu, V. Kumar, and A. K. Ramasamy, "Design & development of compact uniplanar semi-hexagonal ACS fed multi-band antenna for portable system application," *Prog. Electromag. Res. M*, vol. 60, pp. 157–167, 2017.

[40] P. Lotfi, M. Azarmanesh, and S. Soltani, "Rotatable dual band-notched UWB/triple-band WLAN reconfigurable antenna," *IEEE IEEE Antennas Wireless Propag. Lett.*, vol. 12, pp. 104–107, 2013.

[41] L. Kang, H. Wang, X. H. Wang, and X. Shi, "Compact ACS-fed monopole antenna with rectangular SRRs for tri-band operation," *Electron. Lett.*, vol. 50, no. 16, pp. 1112–1114, Jul. 2014.

[42] X. Li, X.-W. Shi, W. Hu, P. Fei, and J.-F. Yu, "Compact triband ACS-fed monopole antenna employing open-ended slots for wireless communication," *IEEE Antennas Wireless Propag. Lett.*, vol. 12, pp. 388–391, 2013.

[43] P. V. Naidu, A. Kumar, and R. Rajkumar, "Design, analysis and fabrication of compact dual band uniplanar meandered ACS fed antenna for 2.5/5 GHz applications," *Microsyst. Technol.*, vol. 25, no. 1, pp. 97–104, 2019.

[44] Y. Wang and L. Jin, "A novel compact ACS-fed UWB antenna with resonators for WiMAX/WLAN applications," in *Proc. 5th Int. Conf. Adv. Mater. Comput. Sci.*, 2016, pp. 222–225.

[45] *Ansys High Frequency Structure Simulator (HFSS)*, Ansys Electromagnetics Suite, Pittsburgh, PA, USA, 2021.

[46] M. Koohestani, A. Hussain, A. A. Moreira, and A. K. Skrivervik, "Diversity gain influenced by polarization and spatial diversity techniques in ultrawideband," *IEEE Access*, vol. 3, pp. 281–286, 2015.

[47] K. S. Ryu and A. A. Kishk, "UWB antenna with single or dual band-notches for lower WLAN band and upper WLAN band," *IEEE Trans. Antennas Propag.*, vol. 57, no. 12, pp. 3942–3950, Dec. 2009.

[48] Keysight Inc. (2022). *Advanced Design System (ADS)*. Santa Rosa, CA, USA. Accessed: Dec. 20, 2022. [Online]. Available: https://www.keysight.com/

[49] F. Zhu, S. Gao, A. T. Ho, R. A. Abd-Alhameed, C. H. See, T. W. Brown, J. Li, G. Wei, and J. Xu, "Multiple band-notched UWB antenna with band-rejected elements integrated in the feed line," *IEEE Trans. Antennas Propag.*, vol. 61, no. 8, pp. 3952–3960, Aug. 2013.

[50] D. Y. Chen and C. F. Wang, *Characteristic Modes: Theory and Applications in Antenna Engineering*. Hoboken, NJ, USA: Wiley, 2015.

[51] D.-L. Wen, Y. Hao, H.-Y. Wang, and H. Zhou, "Design of a wideband antenna with stable omnidirectional radiation pattern using the theory of characteristic modes," *IEEE Trans. Antennas Propag.*, vol. 65, no. 5, pp. 2671–2676, May 2017.

[52] B. B. Q. Elias, P. J. Soh, A. A. Al-Hadi, P. Akkaraekthalin, and G. A. E. Vandenbosch, "A review of antenna analysis using characteristic modes," *IEEE Access*, vol. 9, pp. 98833–98862, 2021.

[53] M. Koohestani, N. Pires, A. K. Skrivervik, and A. A. Moreira, "Band-reject ultra-wideband monopole antenna using patch loading," *Electron. Lett.*, vol. 48, no. 16, pp. 974–975, Aug. 2012.
[54] G. Quintero, J. F. Zürcher, and A. K. Skrivervik, "System fidelity factor: A new method for comparing UWB antennas," *IEEE Trans. Antennas Propag.*, vol. 59, no. 4, pp. 2502–2512, Jul. 2011.
[55] M. Koohestani, J.-F. Zürcher, A. Moreira, and A. Skrivervik, "A novel, low-profile, vertically-polarized UWB antenna for WBAN," *IEEE Trans. Antennas Propag.*, vol. 62, no. 4, pp. 1888–1894, Apr. 2014.
[56] M. Koohestani, A. A. Moreira, and A. K. Skrivervik, "Fidelity concepts used in UWB systems," in *Proc. IEEE Antennas Propag. Soc. Int. Symp. (APSURSI)*, Jul. 2014, pp. 824–825.

MOHSEN KOOHESTANI (Senior Member, IEEE) received the Ph.D. degree (Hons.) in electromagnetics from the École Polytechnique Fédérale de Lausanne (EPFL), Lausanne, Switzerland, and the Universidade de Lisboa (ULISBOA), Lisbon, Portugal, in 2014.

From 2014 to 2018, he was a Senior Research Fellow with the Institute of Electronics and Telecommunications of Rennes (IETR), University of Rennes 1, working mainly on biomedical applications of wireless power transfer systems. He has been an Associate Professor with the ESEO School of Engineering, Angers, France, since 2018. He is currently an Associate Researcher with IETR, UMR CNRS 6164. He has authored or coauthored over 70 peer-reviewed scientific papers. His research interests include domain of antennas, microwaves, EMC, and biomedical engineering.

Dr. Koohestani is an Official Member of the IEC Standardization Working Group (WG2 & WG9) in the SC47A French Subcommittee on the EMC for integrated circuits.

NIMA AZADI-TINAT received the B.Sc. degree from the Amirkabir University of Technology, Tehran, Iran, in 2003, and the M.Sc. and Ph.D. degrees in electrical engineering from the University of Science and Technology, Tehran, in 2008 and 2014, respectively.

In 2014, he joined the Department of Electrical and Robotic Engineering, Shahrood University of Technology, Shahrood, Iran, where he is currently an Assistant Professor. His research interests include antennas, active and passive microwave circuits, and electromagnetic fields propagation theory.

ANJA K. SKRIVERVIK received the master's and Ph.D. degrees in electrical engineering from the Ecole Polytechnique Fédérale de Lausanne (EPFL), Lausanne, Switzerland, in 1986 and 1992, respectively.

She was an Invited Research Fellow with the University of Rennes, Rennes, France, followed by two years in the industry. In 1996, she rejoined EPFL, as an Assistant Professor, where she is currently a Full Professor and also the Head of the Microwave and Antenna Group. Her teaching activities include courses on microwaves and antennas and courses at bachelor's, master's, and Ph.D. levels. She is very active in European collaboration and European projects. She is frequently requested to review research programs and centers in Europe. She has authored or coauthored over 200 peer-reviewed scientific publications. Her current research interests include electrically small antennas, antennas in biological media, multifrequency and ultra-wideband antennas, and numerical techniques for electromagnetics.

Dr. Skrivervik has been a member of the Board of Directors of the European Association on Antennas and Propagation, since 2017. She is a Board Member of the European School on Antennas. She was a recipient of the Latsis Award. She was the Chairperson of the Swiss URSI, until 2012. She was the Director of the EE Section, from 1996 to 2000.